6th European Conference on Computational Mechanics (ECCM 6)
7th European Conference on Computational Fluid Dynamics (ECFD 7)
1115 June 2018, Glasgow, UK

HOMOGENIZATION BASED MODELLING OF THE PERFUSED LIVER TISSUE

EDUARD ROHAN[1], JANA TURJANICOVÁ[1] AND VLADIM IR LUKEŠ[1]

[1] Faculty of Applied Sciences, European Centre of Excellence, NTIS – New Technologies for Information Society, University of West Bohemia, Univerzitní 8, 306 14 Plzeň, Czech Republic, rohan@kme.zcu.cz

Key words: Homogenization, Double Porosity, Liver Tissue, Perfusion

Abstract. We present two different homogenization based approaches to upscaling the liver perfusion at the lobular level. The first one consists in homogenization of the mesoscopic structure with the double-porosity medium represented by the Darcy flow model with large contrasts in the permeability. The second perfusion model is based on the two-level homogenization of the fluid-structure interaction with a scaling ansatz related to the viscosity is applied. Both the models are compared in terms of their macroscopic responses. Beyond the scope of this paper, for both the approaches the corresponding extensions accounting for the tissue deformation have been derived.

1 INTRODUCTION

Understanding of liver perfusion on the multiple scales is crucial for the surgical treatment (liver resections, transplantations), but also for understanding how the liver perfusion is modified by diffuse parenchyma diseases such as cirrhosis, steatohepatitis, or the sinusoidal obstruction syndrome. The liver parenchyma is organized by the lobular structure constituted by the sinusoidal porosity separating the so-called vertex and central veins. Existing studies of the liver microcirculation [3, 2], i.e. perfusion between the portal track and the central vein at lobular level, usually consider the conception of the regular hexagonal liver lobulus as the hepatic functional unit, see e.g. [9, 4].

We have developed two homogenized models relying on different assumptions and upscaling approaches. The first one is derived by the homogenization of the mesoscopic structure with the double-porosity medium represented by the Biot model with large contrasts in the permeability, cf. [1]. In the sinusoidal porosity, the scaling of the permeability leads to the macroscopic model involving two pressure fields associated with the portal and hepatic vascular compartments. The poro-viscoelastic coefficients involved in the time convolution integrals are obtained by the homogenization of the quasistatic Biot model, whereby time convolution integrals yield the fading memory effects. The macroscopic model is featured by the fading memory effects inherited from the time convolution integrals, cf. [5, 6]

The second perfusion model is an extension of our recent work [8], to account for deformations and the 3 compartment mesoscopic topology. Two-level homogenization of the fluid-structure interaction with a scaling ansatz related to the viscosity is applied. The macroscopic model is defined in terms of the pressure field associated with flow in the liver sinusoids, and the two velocity fields associated with the precapillary vessels of the portal and hepatic vein systems. Interface conditions relevant to the mesoscopic scale are obtained along with the mesoscopic model comprising the Darcy flow in the dual (sinusoidal) porosity and the Stokes flow model in the mesoscopic channels (the precapillary vessels of the portal and hepatic venous systems). To consider the influence of deformation of the perfusion, so far this model has been extended for the two-compartment topology only, see [7].

In this paper, we illustrate and compare properties of the two models, the Darcy-Brinkman model and the double-permeability Darcy model, using selected examples with the representative periodic cell describing the lobulus of the liver tissue. A sensitivity study related to the mesoscopic geometry is reported. The numerical results are computed using the FE method implemented in the SfePy software (see `http://sfepy.org`).

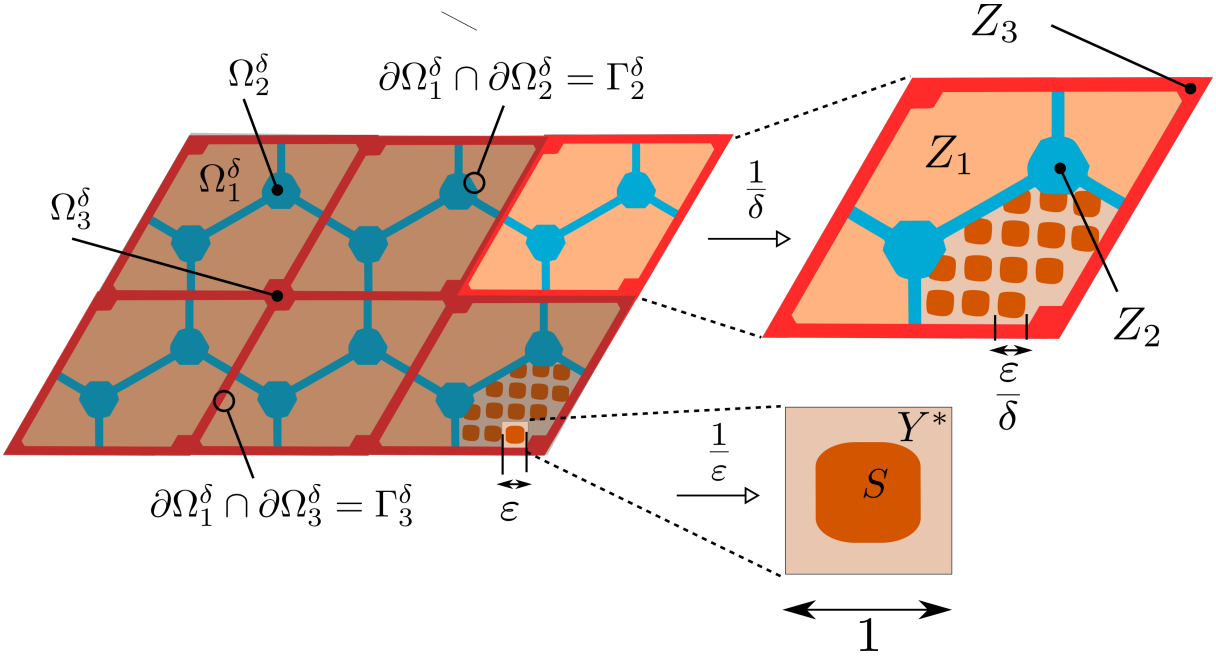

Figure 1: Lobular porous structure parameterized by ε, the characteristic size of the sinusoidal porosity, and δ which describes the size of the mesoscopic heterogeneities.

2 THE DARCY–BRINKMAN MODEL

The model derived in [8] for the two-compartment mesoscopic topology has been extended for three compartments corresponding to the lobular structure.

2.1 Micromodel and two-level homogenization strategy

The hierarchical porous material occupying open bounded domain $\Omega \subset \mathbb{R}^3$ is characterized by two scales related to two small parameters ε and δ, see Fig. 1. At the mesoscopic scale the periodic structure is formed by channels represented by domain Ω_F^δ occupied by fluid, and by the microporous material $\Omega_1^\delta = \Omega \setminus \Omega_F^\delta$. In particular, domain $\Omega_1^{\varepsilon,\delta} \subset \Omega_1^\delta$ represents micro pores occupied by fluid, whereas $S^{\varepsilon,\delta} = \Omega_1^\delta \setminus \Omega_1^{\varepsilon,\delta}$ is the skeleton.

The fluid domain Ω_F^δ is constituted by two mutually disconnected channel systems Ω_2^δ and Ω_3^δ representing the precapillary vasculature, thus $\Omega_F^\delta = \Omega_2^\delta \cup \Omega_3^\delta$. The domain occupied by the fluid is

$$\Omega^{\varepsilon,\delta} = \Omega_1^{\varepsilon,\delta} \cup \Omega_F^\delta \cup \Gamma^\delta \ , \qquad \text{where } \Gamma^\delta = \Omega_1^{\varepsilon,\delta} \cap \Omega_F^\delta \ . \tag{2.1}$$

Obviously $\Gamma^\delta = \Gamma_2^\delta \cup \Gamma_3^\delta$ consist of two disjoint parts, $\Gamma_\beta^\delta = \Omega_1^{\varepsilon,\delta} \cap \Omega_\beta^\delta$, $\beta = 2, 3$.

The micropores form a periodic structure generated by the representative cell εY, whereby $Y =]0,1[^3$ (in general, Y can be a parallelepiped in $\mathbb{R}^3$) and ε is proportional to the size of pores. Y is decomposed into the solid part $S \subset \overline{Y}$ and the fluid part $Y^* = Y \setminus S$, thus $S^{\varepsilon,\delta}$ is generated as the periodic lattice by the representative skeleton εS. At the mesoscopic level the structure is generated by the periodic cell δZ, where $Z =]0,1[^3$ is constituted by microporous part situated in $Z_1 \subset Z$ and by the fluid part $Z_F = Z \setminus Z_1$; as an extension to work [8] we consider two subdomains $Z_\beta \subset Z_F$, $\beta = 2, 3$, such that $Z_2 \cap Z_3 = \emptyset$ and $Z_F = Z_2 \cup Z_3$; further, by $\Gamma_Z = \overline{Z_1} \cap \overline{Z_F}$ we denote the interface consisting of two disjoint parts, $\Gamma_Z = \Gamma_Z^2 \cup \Gamma_Z^3$. This decomposition of the representative cell at the mesoscopic level (the lobular level) will be adopted in Section 3

2.2 Micromodel and the high contrast in the fluid viscosity

The size of the channels (mesoscopic pores) is proportional to δ. For given scale parameters ε and δ, the flow of an incompressible viscous fluid is described by the Stokes problem governed by the following equations:

$$\begin{aligned} -\nabla \cdot \left(\mu^{\varepsilon,\delta} \boldsymbol{e}(\boldsymbol{u}^{\varepsilon,\delta}) - p^{\varepsilon,\delta}\right) &= \boldsymbol{f} \ , \quad \text{in } \Omega_1^{\varepsilon,\delta} \cup \Omega_F^\delta \ , \\ \boldsymbol{u}^{\varepsilon,\delta} &= 0 \ , \quad \text{on } \partial S^{\varepsilon,\delta} \cup \partial\Omega \ , \\ \nabla \cdot \boldsymbol{u}^{\varepsilon,\delta} &= 0 \ , \quad \text{in } \Omega_1^{\varepsilon,\delta} \cup \Omega_F^\delta \ , \end{aligned} \tag{2.2}$$

where $\boldsymbol{u}^{\varepsilon,\delta}$ is the fluid velocity, $\boldsymbol{e}(\boldsymbol{u}^{\varepsilon,\delta}) = 0.5(\nabla \boldsymbol{u}^{\varepsilon,\delta} + (\nabla \boldsymbol{u}^{\varepsilon,\delta})^T)$ is the velocity strain, $p^{\varepsilon,\delta}$ is the pressure, and the viscosity $\mu^{\varepsilon,\delta}$ is given by piece-wise constant function according the micropore size ε:

$$\mu^{\varepsilon,\delta} = \begin{cases} \varepsilon^2 \mu_1 & \text{in} \quad \Omega_1^{\varepsilon,\delta} \ , \\ \mu_F & \text{in} \quad \Omega_F^\delta \ . \end{cases} \tag{2.3}$$

2.3 The mesoscopic model

The mesoscopic flow is governed by the following equations obtained by the asymptotic analysis ($\varepsilon \to 0$, whereas δ being fixed, see [8]) of the system (2.2) with the viscosity (2.3),

$$\begin{aligned} -\nabla \cdot \mu_1^{-1} \boldsymbol{K}(\nabla p_1 - \boldsymbol{f}) = 0 \,, \quad & \text{in } \Omega_1 \,, \\ -\mu_F \nabla^2 \boldsymbol{u}_\beta + \nabla p_\beta = f \,, \quad & \text{in } \Omega_\beta \,, \quad \beta = 2,3 \,, \\ \nabla \cdot \boldsymbol{u}_\beta = 0 \,, \quad & \text{in } \Omega_\beta \,, \\ \boldsymbol{u}_\beta = 0 \,, \quad & \text{on } \partial\Omega \,, \\ \boldsymbol{n}^{[1]} \cdot \boldsymbol{u}_1 := -\mu_1^{-1} \boldsymbol{K}(\nabla p_1 - \boldsymbol{f}) \cdot \boldsymbol{n}^{[1]} = -\boldsymbol{n}^{[\beta]} \cdot \boldsymbol{u}_2 \,, \quad & \text{on } \Gamma \,, \\ \boldsymbol{n}^{[\beta]} \cdot (\mu_F \boldsymbol{e}(\boldsymbol{u}_\beta) - p_\beta) = -p_1 \boldsymbol{n}^{[\beta]} \,, \quad & \text{on } \Gamma_\beta \,, \end{aligned} \tag{2.4}$$

where $\boldsymbol{u}_1 = -\mu_1^{-1} \boldsymbol{K}(\nabla p_1 - \boldsymbol{f})$ is the mesoscopic flow in the microporosity. Hence we obtain the interface conditions on Γ; the following conditions are deduced from $(2.4)_{5,6}$,

$$\begin{aligned} \boldsymbol{n}^{[\beta]} \cdot (\boldsymbol{u}_\beta - \boldsymbol{u}_1) = 0 \,, \quad \beta = 2,3 \,, \\ p_\beta - p_1 = \mu_F \boldsymbol{e}(\boldsymbol{u}_\beta) : \boldsymbol{n}^{[\beta]} \otimes \boldsymbol{n}^{[\beta]} \,, \\ \boldsymbol{t} \cdot \partial_n \boldsymbol{u}_\beta + \boldsymbol{n} \cdot \partial_t \boldsymbol{u}_\beta = 0 \,, \end{aligned} \tag{2.5}$$

denoting by $\boldsymbol{t}$ a unit vector in the tangential plane of Γ, *i.e.* $\boldsymbol{n} \cdot \boldsymbol{t} = 0$, where $\partial_n = \boldsymbol{n} \cdot \nabla$ and $\partial_t = \boldsymbol{t} \cdot \nabla$. It is worth to note that this condition is obtained as the byproduct of the 1st level homogenization step without any restriction on the curvature of Γ.

2.4 The 2nd level homogenization

The macroscopic model of the perfusion is obtained by the asymptotic analysis with respect to the characteristic scale $\delta \to 0$ of the mesoscopic problem (2.4). Below we present the local problems for characteristic responses which constitute the homogenized coefficients involved in the macroscopic problem. The resulting equations and expressions were obtained using the approach developed in [8].

2.4.1 Local mesoscopic problems

The following autonomous problems are imposed in the two parts of the mesoscopic representative volume: problem (2.6) describes the characteristic pressure response of the sinusoidal porosity, while the problems (2.7) provide the characteristic flow in the portal and hepatic precapillary channels.

- Find $\pi^k, \psi^{k,\beta} \in H^1_\#(Z_1)/\mathbb{R}$, such that

$$\begin{aligned} \int_{Z_1} \frac{1}{\mu_1} \boldsymbol{K} \nabla_z \pi^k \cdot \nabla_z q = -\int_{Z_1} \frac{1}{\mu_1} \boldsymbol{K} \nabla_z z_k \cdot \nabla_z q \,, \quad \forall q \in H^1_\#(Z) \,, \\ \int_{Z_1} \frac{1}{\mu_1} \boldsymbol{K} \nabla_z \psi^{k,\beta} \cdot \nabla_z q = \int_{Z_\beta} \partial^z_k q = -\int_{\Gamma^\beta_Z} n^{[1]}_k q \,, \quad \forall q \in H^1_\#(Z) \,, \end{aligned} \tag{2.6}$$

- Find $\boldsymbol{w}^{ij,\beta} \in \tilde{\mathbf{H}}^1_{\#}(Z_\beta)$, $\hat{\pi}^{ij,\beta} \in L^2(Z_\beta)$ such that

$$\begin{aligned} \fint_{Z_\beta} \mu_\beta \boldsymbol{e}_z(\boldsymbol{w}^{ij,\beta} + \boldsymbol{\Pi}^{ij}) : \boldsymbol{e}_z(\boldsymbol{v}) - \fint_{Z_\beta} \hat{\pi}^{ij,\beta} \nabla_z \cdot \boldsymbol{v} = 0 \ , \quad \forall \boldsymbol{v} \in \mathbf{H}^1_{\#}(Z_\beta) \ , \\ \fint_{Z_\beta} \nabla_z \cdot \left(\boldsymbol{w}^{ij,\beta} + \boldsymbol{\Pi}^{ij}\right) q = 0 \ , \quad \forall q \in L^2(Z_\beta) \ , \end{aligned} \tag{2.7}$$

  where $\boldsymbol{\Pi}^{ij} = (\Pi^{ij}_k)$ with $\Pi^{ij}_k = z_j \delta_{ik}$.

2.4.2 Macroscopic problem

The homogenized coefficients involved in the macroscopic problem are computed using the characteristic responses ($i,j,k,l = 1,2,3$ and $\beta, \alpha = 2,3$),

$$\begin{aligned} \mathcal{C}_{ij} &= \fint_{Z_1} [\frac{1}{\mu_1} \boldsymbol{K} \nabla_z (z_j + \pi^j)] \cdot \nabla_z (z_i + \pi^i) \ , \\ \mathcal{P}^\beta_{lk} &= \phi_\beta \delta_{kl} - \fint_{Z_1} [\frac{1}{\mu_1} \boldsymbol{K} \nabla_z \psi^{k,\beta}]_l \ , \\ \mathcal{P}^{\beta *}_{lk} &= \phi_\beta \delta_{kl} + \fint_{Z_\beta} \partial^z_l \pi^k = \phi_\beta \delta_{kl} + \fint_{\Gamma^\beta_Z} n^{[\beta]}_l \pi^k = \phi_2 \delta_{kl} - \fint_{Z_1} \partial^z_l \pi^k \ , \\ \mathcal{A}^\beta_{ijkl} &= \fint_{Z_\beta} \mu_\beta \boldsymbol{e}_z(\boldsymbol{\Pi}^{kl} + \boldsymbol{w}^{kl,\beta}) : \boldsymbol{e}_z(\boldsymbol{\Pi}^{ij} + \boldsymbol{w}^{ij,\beta}) \ , \\ \mathcal{H}^{\alpha\beta}_{kl} &= \fint_{Z_\alpha} (\nabla_z \psi^{l,\beta})_k = \fint_{Z_1} [\frac{1}{\mu_1} \boldsymbol{K} \nabla_z \psi^{k,\alpha}] \cdot \nabla_z \psi^{l,\beta} \ , \end{aligned} \tag{2.8}$$

The symmetry $\mathcal{P}^{*\beta}_{kl} = \mathcal{P}^\beta_{lk}$ can be proved, as in [8].

By virtue of the Stokes flow two-level homogenization, the macroscopic model of the lobular structure involves two velocity fields associated with the portal and hepatic vein channels, and the pressure related to the sinusoidal porosity. The weak formulation reads, as follows: Find $(p^0, \boldsymbol{u}^2, \boldsymbol{u}^3) \in H^1(\Omega) \times \mathbf{H}^1_0(\Omega) \times \mathbf{H}^1_0(\Omega)$ such that

$$\begin{aligned} \int_\Omega [\boldsymbol{\mathcal{C}} \nabla p^0 - \sum_\beta \boldsymbol{\mathcal{P}}^\beta \boldsymbol{u}^\beta] \cdot \nabla q = \int_\Omega [\boldsymbol{\mathcal{C}} \boldsymbol{f}] \cdot \nabla q \ , \quad \forall q \in H^1(\Omega) \ , \\ \int_\Omega [\boldsymbol{\mathcal{A}}^\alpha \boldsymbol{e}(\boldsymbol{u}^\alpha)] : \boldsymbol{e}(\boldsymbol{v}) + \int_\Omega [(\boldsymbol{\mathcal{P}}^\alpha)^T \nabla p^0] \cdot \boldsymbol{v} + \sum_\beta \int_\Omega \boldsymbol{v} \cdot \boldsymbol{\mathcal{H}}^{\alpha\beta} \boldsymbol{u}^\beta = \int_\Omega [(\boldsymbol{\mathcal{P}}^\alpha)^T \boldsymbol{f}] \cdot \boldsymbol{v} \ , \quad \forall \boldsymbol{v} \in \mathbf{H}^1_0(\Omega) \ , \\ \int_\Omega p^0 = 0 \ . \end{aligned} \tag{2.9}$$

If the microporosity $\Omega^{\varepsilon,\delta}$ is a connected domain, thus Z_1 and Y^* are connected, $\boldsymbol{\mathcal{C}}$ is positive definite. If Ω^δ_β are connected domains, $\boldsymbol{\mathcal{A}}^\beta$ are positive definite and so also $\boldsymbol{\mathcal{H}}^{\beta\beta}$, $\beta = 2,3$.

2.4.3 Macroscopic model

From (2.8), it is straightforward to obtain the strong formulation for which the boundary conditions can be generalized: Find unknown fields $(p^0, \boldsymbol{u}^2, \boldsymbol{u}^3)$ which satisfy

$$\begin{aligned} -\nabla\cdot[\boldsymbol{\mathcal{C}}(\nabla p^0 - \boldsymbol{f}) - \sum_\beta \boldsymbol{\mathcal{P}}^\beta \boldsymbol{u}^\beta] = 0\ ,\ \text{in}\ \Omega\ , \\ -\nabla\cdot[\boldsymbol{\mathcal{A}}^\alpha \boldsymbol{e}(\boldsymbol{u}^\alpha)] + (\boldsymbol{\mathcal{P}}^\alpha)^T(\nabla p^0 - \boldsymbol{f}) + \sum_\beta \boldsymbol{\mathcal{H}}^{\alpha\beta}\boldsymbol{u}^\beta = 0\ \text{in}\ \Omega\ ,\quad \alpha = 2,3\ . \end{aligned} \tag{2.10}$$

with the boundary conditions ($\boldsymbol{n}\cdot\boldsymbol{t} = 0$, whereby $\boldsymbol{t}$ is any tangent) :

$$\begin{aligned} \boldsymbol{n}\cdot\boldsymbol{u}^\alpha &= \bar{u}_n^\alpha \quad \text{on}\ \partial\Omega\ , \\ \boldsymbol{n}\otimes\boldsymbol{t} : \boldsymbol{\mathcal{A}}^\alpha \boldsymbol{e}(\boldsymbol{u}^\alpha) &= \bar{\sigma}_t^\alpha \quad \text{on}\ \partial\Omega\ , \\ p^0 &= \bar{p} \quad \text{on}\ \partial_p\Omega\ , \\ \boldsymbol{n}\cdot(\boldsymbol{\mathcal{C}}\nabla p^0 - \sum_\beta \boldsymbol{\mathcal{P}}^\beta \boldsymbol{u}^\beta) &= \bar{w} \quad \text{on}\ \partial_w\Omega\ , \end{aligned} \tag{2.11}$$

where $\partial\Omega = \partial_p\Omega \cup \partial_w\Omega$ and these parts are disjoint, $\partial_p\Omega \cup \partial_w\Omega = \emptyset$. In Section 4 we present an example in which the boundary conditions were prescribed according (2.11).

3 THE TWO-COMPARTMENT DARCY FLOW MODEL

The second model which can be used for modelling the tissue perfusion is based on the Darcy flow with the double porosity. In [6] the model was derived assuming the tissue deformability. Here we present the mode for a rigid skeleton. The domain Ω is decomposed according to (2.1), however, the dual porosity is already homogenized; the only scale parameter δ is related to the mesoscopic scale, thus, $\Omega^\delta = \Omega_1^\delta \cup \Omega_F^\delta \cup \Gamma^\delta$,

3.1 The mesoscopic model — lobular level

At the mesoscopic level, reference periodic cell Z is identical with the one employed for the first model, see Section 2.1. The permeability in the dual porosity is proportional to δ^2, such that

$$\boldsymbol{D}^\delta = \begin{cases} \delta^2 \bar{\boldsymbol{D}}^{1,\delta} & \text{in}\quad \Omega_1^\delta\ , \\ \boldsymbol{D}^{\beta,\delta} & \text{in}\quad \Omega_\beta^\delta,\ \beta = 2,3\ , \end{cases} \tag{3.1}$$

whereby there exist constants $\underline{c}, \overline{c} > 0$ such that $\underline{c}|\boldsymbol{D}^{\alpha,\delta}| \le |\bar{\boldsymbol{D}}^{1,\delta}| \le \overline{c}\boldsymbol{D}^{\beta,\delta}|$ for $\alpha,\beta \in \{2,3\}$. The mesoscopic Darcy flow is governed by the following system of equations,

$$\left.\begin{aligned} \nabla\cdot\boldsymbol{w}^\delta &= 0\ , \\ \boldsymbol{w}^\delta &= -\boldsymbol{D}^\delta(\nabla p^\delta - \boldsymbol{f}^\delta)\ , \end{aligned}\right\} \quad \text{in}\ \Omega_1^\delta \cup \Omega_2^\delta \cup \Omega_3^\delta\ , \tag{3.2}$$

where the obvious interface pressure and flux continuity is prescribed, $[p^\delta]_\beta^1 = 0$ and $[\boldsymbol{w}^\delta\cdot\boldsymbol{n}]_\beta^1 = 0$, $\beta = 1,2$

$$\boldsymbol{n}\cdot\boldsymbol{w}^\delta = g^\delta = \begin{cases} \delta\bar{g}^1 & \text{in}\quad \partial_{\text{ext}}\Omega_1^\delta\ , \\ g^\beta & \text{in}\quad \partial_{\text{ext}}\Omega_\beta^\delta,\ \beta = 2,3\ . \end{cases} \tag{3.3}$$

The effective flow model presented in the subsequent sections has been derived from the weak formulation of (3.2)-(3.3). Below we present only the local and global (macroscopic) models.

3.2 The local problems

Two local problems for the characteristic responses must be solved in domain Z.

- The characteristic response in the dual porosity (smeared sinusoids) expresses the flow through the porosity Z_1 due to the unit pressure difference between the two interfaces. We define $H^1_{\#0}(Z_1) = \{\psi \in H^1_{\#}(Z_1)|\ , \psi = 0 \text{ on } \Gamma_Z\}$ and consider function $\bar\varphi \in H^1_{\#}(Z_1)$ such that $\bar\varphi = 1$ on Γ^1_Z and $\bar\varphi = 0$ on Γ^2_Z. The problem reads: Find $\tilde\varphi_1 \in H^1_{\#0}(Z_1)$ such that

$$\int_{Z_1} [\bar{\boldsymbol{D}}^1 \nabla(\tilde\varphi_1 + \bar\varphi_1)] \cdot \nabla\psi = 0 \quad \text{for all } \psi \in H^1_{\#0}(Z_1)\ , \tag{3.4}$$

- The second characteristic response describes the flow induced by a unit macroscopic pressure gradient in the portal and hepatic channels: Find $\tilde\varphi_\beta \in \tilde H^1_{\#}(Z_\beta)$ such that

$$\int_{Z_\beta} [\boldsymbol{D}^\beta \nabla(\varphi^i_\beta + z^i)] \cdot \nabla\psi = 0 \quad \text{for all } \psi \in H^1_{\#}(Z_\beta)\ ,\ \beta = 2,3\ . \tag{3.5}$$

3.3 The macroscopic model

Using the solutions of (3.4) and (3.5), the macroscopic flow coefficients are computed by two volume integrals,

$$\begin{aligned} K^\beta_{ij} &= \frac{1}{|Y|}\int_{Y_d} [\boldsymbol{D}^\beta \nabla(\varphi^i_\beta + z^i)] \cdot \nabla(\varphi^j_\beta + z^j) = 0\ , \quad \beta = 2,3\ , \\ G &= \frac{1}{|Y|}\int_{\Gamma_2} \boldsymbol{\nu} \cdot [\boldsymbol{D}_m \nabla(\tilde\varphi_1 + \bar\varphi_1)]\ . \end{aligned} \tag{3.6}$$

The macroscopic flow in the precapillary porosities of the lobulae is governed problem describing distribution of the two macroscopic pressures, $p^\alpha \in \tilde H^1(\Omega)$, $\alpha = 2,3$,

$$\int_\Omega [\boldsymbol{K}^\alpha(\nabla p^\alpha - \bar{\boldsymbol{f}}^\alpha)] \cdot \nabla q^\alpha + \int_\Omega G(p^\alpha - p^\beta) q^\alpha = \int_{\partial\Omega} \bar g^\alpha q^\alpha\ , \quad \text{for all } q^\alpha \in H^1(\Omega)\ , \alpha \neq \beta \tag{3.7}$$

where $\bar g^\alpha = \bar\phi^\alpha g^\alpha$ and $\bar{\boldsymbol{f}}^\alpha = \phi^\alpha \boldsymbol{f}^\alpha$ are defined using the volume and surface porosities, respectively, ϕ^α and $\bar\phi^\alpha$.

From (3.7), the strong formulation can be expressed easily:

$$\begin{aligned} -\nabla \cdot [\boldsymbol{K}^\alpha(\nabla p^\alpha - \bar{\boldsymbol{f}}^\alpha)] + G(p^\alpha - p^\beta) = 0 \quad &\text{in } \Omega\ , \quad \alpha = 2,3\ , \alpha \neq \beta \\ \boldsymbol{n} \cdot \boldsymbol{K}^\alpha(\nabla p^\alpha - \bar{\boldsymbol{f}}^\alpha) = \bar g^\alpha \quad &\text{on } \partial\Omega\ , \quad \alpha = 2,3\ . \end{aligned} \tag{3.8}$$

Below we shall assume that all the volume forces are zero, $\bar{\boldsymbol{f}}^\alpha = \boldsymbol{0}$.

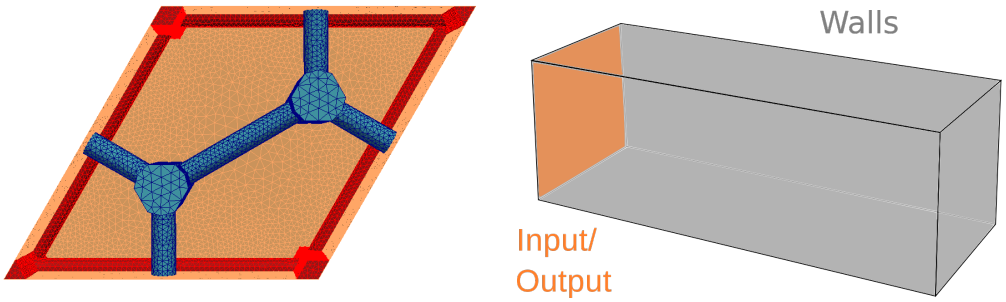

Figure 2: Left: Geometry representation of microscale; subdomains indicated. Right: Geometric representation of a macroscopic tissue specimen; boundary parts indicated.

4 NUMERICAL EXAMPLES

The two models presented in Sections 2 and 3 has been used to simulate flows in the periodic lobular structure of the liver, which is generated using the RPC shown in Fig. **??**. Here we aim to compare both the homogenized models which, at the lobular level, describe flow in the sinusoidal porosity by the Darcy flow model. The sinusoids distributed in Z_1 form a microporosity characterized by a highly anisotropic permeability $\boldsymbol{D}^1$ which reflects the blood flow in the capillary network. Since the Darcy flow model is relevant to both the mesoscopic models (2.4) and (3.2), in domain Ω_1^δ with the RPC Z_1 we use the results of [3, 2], from where the permeability tensors can be reconstructed locally with respect to the cylindrical system established with its axis aligned with the central vein.

It should be emphasized that in (2.4) the permeability $\mu_1^{-1}\boldsymbol{K}$ is the result of the first level homogenization and involves the viscosity $\varepsilon_0^2\mu_1$ established for a given characteristic size of the capillary porosity. For the second model, in (3.1), the permeability is assumed to be given, therefore, we can relate the two models by $\delta_0^2\bar{\boldsymbol{D}}^{1,\delta} \approx (\varepsilon_0^2\mu_1)^{-1}\boldsymbol{K}$, for a given mesoscopic characteristic length, *i.e.* the scale parameter $\delta_0 = 10^{-2}$, while the blood viscosity $\varepsilon_0^2\mu_1 = 1.0 \times 10^{-3}$Pa.s, thus μ_1 is evaluated for the sinusoidal porosity characteristic size, $\varepsilon_0 \approx 10^{-4}$.

symbol	quantity	value	unit
k_r	radial permeability	1.6×10^{-14}	m^2
k_ϕ	tangential permeability	1.8×10^{-14}	m^2
k_z	axial permeability	3.6×10^{-14}	m^2
$\varepsilon_0^2\mu_1$	real viscosity	1.0×10^{-3}	Pa.s
μ_F	viscosity in canals	1.25×10^{-3}	Pa.s
ε_0	scale parameter	1.0×10^{-4}	-
δ_0	scale parameter	1.0×10^{-2}	-

Table 1: Model parameter values.

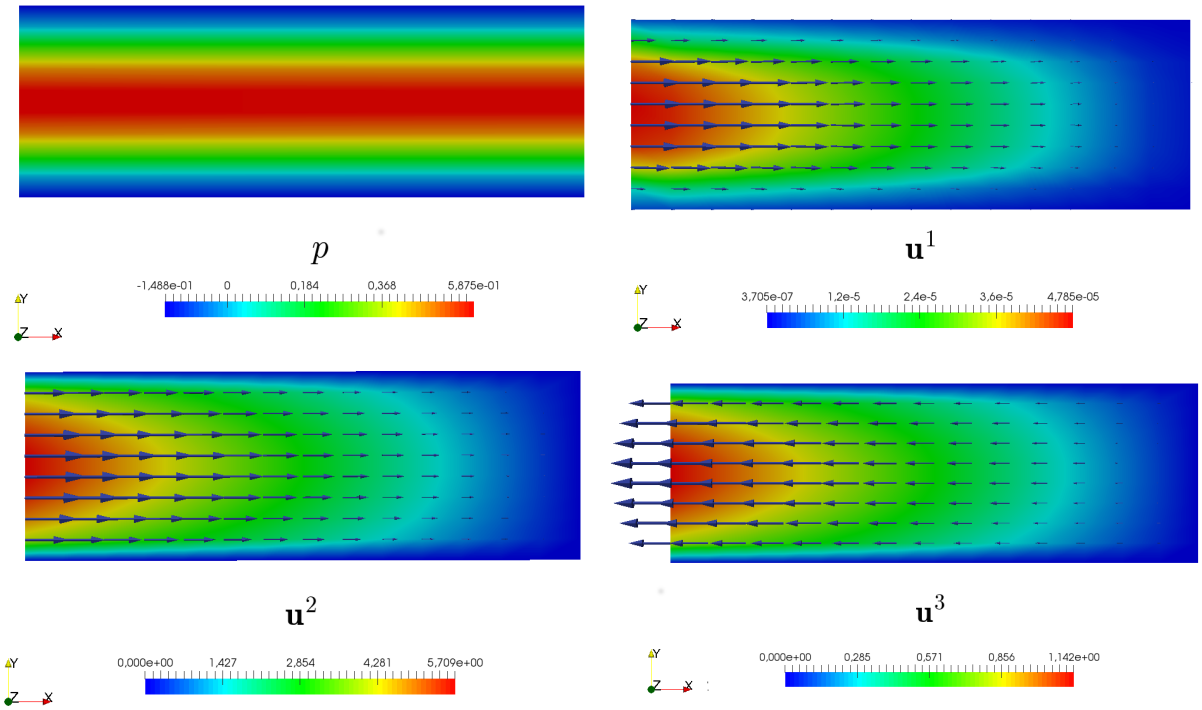

Figure 3: The response $(p, \boldsymbol{u}^2, \boldsymbol{u}^3)$ of the Darcy-Brinkman model, reconstructed velocity $\boldsymbol{u}^1$ in the microporosity.

4.1 The Darcy-Brinkman model

As mentioned above, here we skip the upscaling procedure at the microscopic level related to the sinusoids. Permeability in the homogenized sinusoidal porosity occupying domain Z_1 are introduced by virtue of works published in [3, 2], see Tab. 1 To upscale the flow at the mesoscopic level, we consider the geometry of the RPC describing the idealized lobular structure, see Fig. 2(left). The local problems (2.6) in the dual porosity Z_1, and (2.7) in Z_β, $\beta = 2, 3$ are solved with the viscosity $\mu_F = 1.25 \times 10^{-2}$ Pa.s.

On the boundary $\partial\Omega$ of the macroscopic hexahedron shaped domain Ω, see the notation in Fig. 2(right), the condition of the type (2.11) are prescribed on Walls: $\bar{u}_n^\alpha = 0$, $\alpha = 2, 3$, on the Input/Output part: $\bar{u}_n^2$ is given, whereby $\bar{u}_n^3 = -0.2\bar{u}_n^2$. In addition, on the whole $\partial\Omega$ we consider $\bar{\sigma}_t^\alpha = 0$, $\alpha = 2, 3$, and require $\int_\Omega p = 0$.

Macroscopic distributions p, $\boldsymbol{u}^2$ and $\boldsymbol{u}^3$ are illustrated in Fig. 3, showing inflow through system of mesoscopic channels Z_2 and outflow through the system of channels Z_3. The fluid is filtered through the microporosity Z_1. The macroscopic pressure distribution of p in the microporosity seems to be constant alongside x_1-axis direction. The velocity field in the microporosity $\boldsymbol{u}^1$ is reconstructed by the Darcy law using p.

4.2 The Double-permeability Darcy model

For the two-compartment Darcy flow model, the sinusoids distributed in Z_1 form a microporosity characterized by a highly anisotropic permeability $\boldsymbol{D}^1$; this has been intro-

duced according the results of [3, 2], as discussed above, see Tab. 1.

Also in the precapillary vessels represented by channels Z_2 and Z_3, the flow is described approximately by the diffusion equations with the permeabilities $\boldsymbol{D}^2$ and $\boldsymbol{D}^3$ which are established as an approximation of the Poiseuille-Stokes flow. Since the precapillary vessels of both the PV (vertex veins) and HV (central veins) systems are defined as cylindrical tubes, the axial permeability can be established by $\bar{K}^{i,\alpha} = \pi R_i^2(z)/8\mu_2$ for any i-the vessel of the two systems ($\alpha = 2, 3$) within domains Z_α. Then, in the i-th vessel $Z_{i,\alpha} \subset Z_\alpha$ involved in Z_α, the permeability is defined by

$$\boldsymbol{K}^{i,\alpha}(z) = \bar{K}^{i,\alpha}\boldsymbol{\nu}^i \otimes \boldsymbol{\nu}^i + \kappa \boldsymbol{I} \ , \quad z \in Z_{i,\alpha} \ ,$$

where $\boldsymbol{\nu}^i \otimes \boldsymbol{\nu}^i$ is the rank-one tensor generated by the vessel axial direction $\boldsymbol{\nu}^i$, while $\kappa\boldsymbol{I}$ is the isotropic permeability part given for a small regularization parameter κ. In the vessel overlaps, for $z \in \bigcap_i Z_{i,\alpha}$, an average of $\boldsymbol{K}^{i,\alpha}$ computed for each i is taken (we drop the details here). With so established permeabilities, the local problems (3.4) in the dual porosity Z_1, and (3.5) in Z_β, $\beta = 2, 3$ are solved.

The boundary conditions considered in problem (3.8) are, as follows: Walls: $\bar{g}^\alpha = 0$, for $\alpha = 2, 3$; Input/Output: $\bar{g}^2$ is given, whereas $\bar{g}^3 = -0.2\bar{g}^2$. In addition, we require $\int_\Omega p^2 = 0$. In Fig. 4, the macroscopic distribution of pressure fields p^2 and p^3 is displayed. The velocity fields $\boldsymbol{u}^2$ and $\boldsymbol{u}^3$ are computed from pressure fields p^2 and p^3 using the Darcy law. We observe qualitatively similar behavior as the one of the Darcy-Brinkman model.

5 CONCLUSIONS

We compared two different models describing flows in the double porous medium which corresponds to an idealized liver tissue. The Darcy-Brinkman model derived in for the two-compartment mesoscopic topology has been extended here for the three compartments corresponding to the sinusoidal porosity and two precapillary venous systems. This model is obtained by the two-level homogenization of Stokes flows with the contrast in the fluid viscosity. The double permeability Darcy flow model has been adapted according to work [6] where the dual porosity scaling proposed in [1] was employed. To describe the liver tissue perfusion, we proposed a geometric model of the periodic lobular structure, based on the representative periodic cell which is associated with the primary lattice defined by the central hepatic veins.

The two models provide solutions of either the pressure or the velocity distributions associated with the mesoscopic porosities constituted by the portal and hepatic venulae. While the Darcy-Brinkman (DB) model provides also the sinusoidal pressure as the macroscopic quantity, in the double-permeability Darcy (DD) model, the microporosity pressure must be reconstructed using the characteristic mesoscopic responses. Qualitatively, in the presented example, the velocity fields computed using both the models are similar. The differences (see Fig. 5) are related to different treatment of the mesoscopic interface conditions the interface between the mesoscopic channels and the sinusoidal porosity.

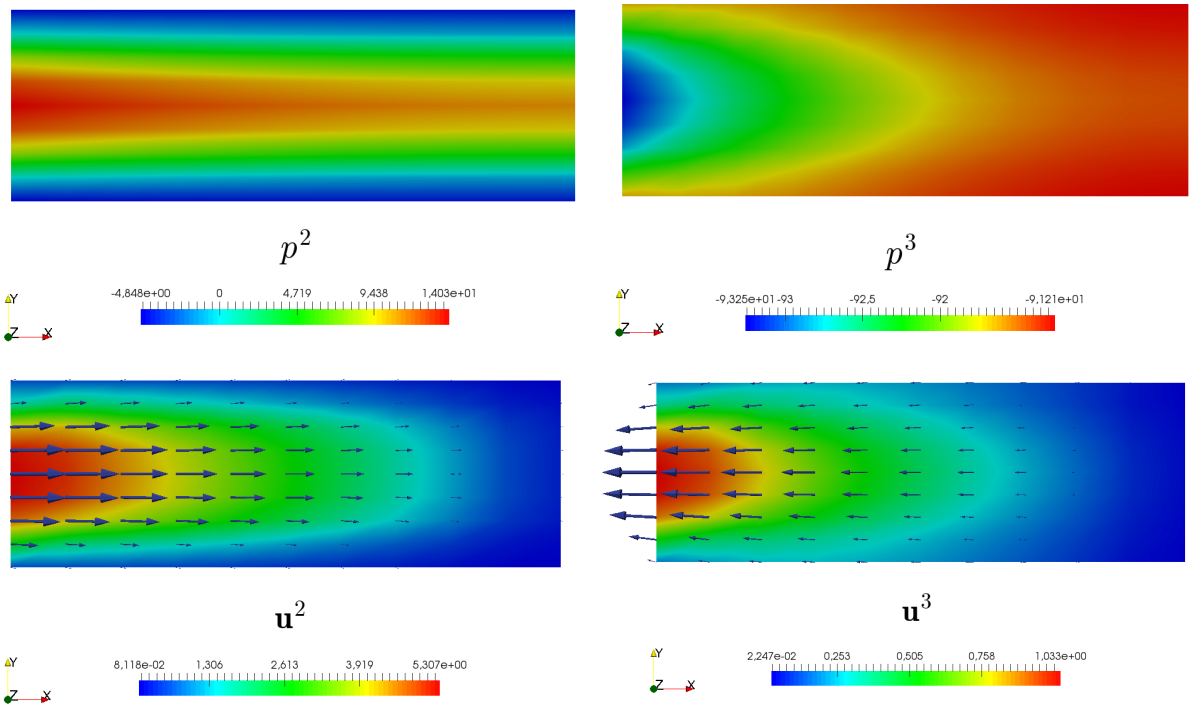

Figure 4: The response (p^2, p^3) of the double-permeability Darcy model; reconstructed velocity $(\boldsymbol{u}^2, \boldsymbol{u}^3)$.

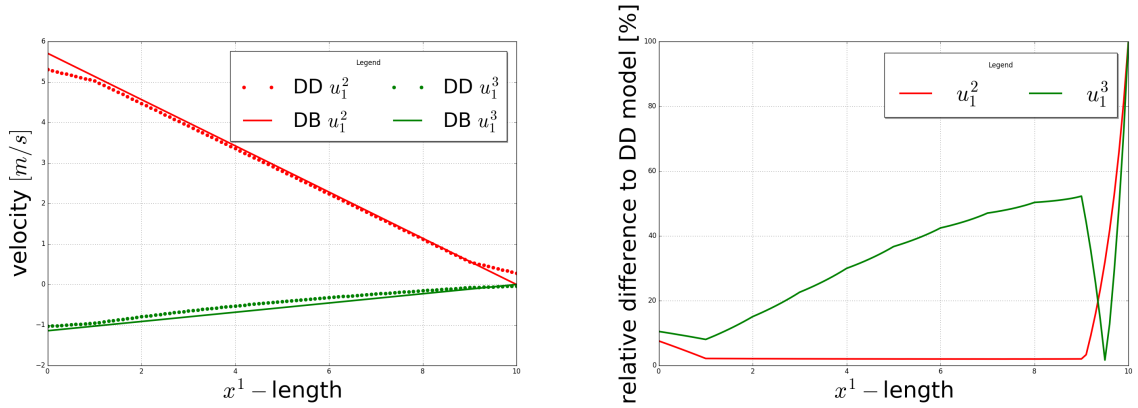

Figure 5: Left: Comparison of the first components of macroscopic velocity fields $(\boldsymbol{u}^2, \boldsymbol{u}^3)$, distribution along x^1-axis for Darcy-Brinkman model (DB) and Double-permeability Darcy model (DD). Right: Differences in velocities $(\boldsymbol{u}^2, \boldsymbol{u}^3)$ obtained as the DB model solution relatively to the DD solution. Note that the highest relative difference is attained for very small velocities.

Acknowledgement. This research is supported by the project LO 1506 of the Czech Ministry of Education, Youth and Sports and in part by GACR 16-03823S of the Czech Scientific Foundation.

REFERENCES

[1] Arbogast, T., Douglas, Jr, J. and Hornung, U. Derivation of the double porosity model of single phase flow via homogenization theory. *SIAM J. Math. Anal.* (1990) **21**(4):823–836.

[2] Debbaut, C., Segers, P., Cornillie, P., Casteleyn, C., Dierick, M., Laleman, W. and Monbaliu, D. Analyzing the human liver vascular architecture by combining vascular corrosion casting and micro-CT scanning: a feasibility study. *J. Anat.* (2014) **224**(4):509–517.

[3] Debbaut, C., Vierendeels, J., Casteleyn, C., Cornillie, P., Van Loo, D., Simoens, P., Van Hoorebeke, L., Monbaliu, D. and Segers, P. Perfusion characteristics of the human hepatic microcirculation based on three-dimensional reconstructions and computational fluid dynamic analysis. *J.Biomech. Eng.* (2012) **134**(1):011003.

[4] Ricken, T., Dahmen, U. and Dirsch, O. A biphasic model for sinusoidal liver perfusion remodeling after outflow obstruction. *Biomechanics and modeling in mechanobiology* (2010) **9**(4):435–450.

[5] Rohan, E., Naili, S., Cimrman, R. and Lemaire, T. Multiscale modeling of a fluid saturated medium with double porosity: Relevance to the compact bone. *J. Mech. Phys. Solids* (2012) **60**(5):857–881.

[6] Rohan, R. and Cimrman, R. Two-scale modeling of tissue perfusion problem using homogenization of dual porous media. *Int. J. Multiscale Comput. Eng.* (2010) **8**(1):81–102.

[7] Rohan, E., Lukeš, V., Turjanicová, J. and Cimrman, R. Two level homogenization of flows in deforming double porosity media: Biot-Darcy-Brinkman model. *In Proceedings of the XIV International Conference on Computational Plasticity (COMPLAS).* Barcelona, CIMNE, 2017. p 184. ISBN: 978-84-946909-6-9.

[8] Rohan, R., Turjanicová, J., and Lukeš, V.A Darcy-Brinkman model of flow in double porous media – two-level homogenization and computational modelling. *To appear in Comput. Struct.* (2018).

[9] Siggers, J.-H., Leungchavaphongse, K., Ho, C.-H. and Repetto, R. Mathematical model of blood and interstitial flow and lymph production in the liver. *Biomechanics and modeling in mechanobiology* (2014) **13**(2):363–378.